NASA Contractor Report 202313
ICOMP–96–12

A Least-Squares Finite Element Method for Electromagnetic Scattering Problems

Jie Wu and Bo-nan Jiang
Institute for Computational Mechanics in Propulsion
Cleveland, Ohio

December 1996

Prepared for
Lewis Research Center
Under Cooperative Agreement NCC3–483

National Aeronautics and
Space Administration

A Least-Squares Finite Element Method for Electromagnetic Scattering Problems

Jie Wu and Bo-nan Jiang
Institute for Computational Mechanics in Propulsion*
NASA Lewis Research Center
Cleveland, OH 44135

Abstract

The least-squares finite element method (LSFEM) is applied to electromagnetic scattering and radar cross section (RCS) calculations. In contrast to most existing numerical approaches, in which divergence-free constraints are omitted, the LSFEM directly incorporates two divergence equations in the discretization process. The importance of including the divergence equations is demonstrated by showing that otherwise spurious solutions with large divergence occur near the scatterers. The LSFEM is based on unstructured grids and possesses full flexibility in handling complex geometry and local refinement. Moreover, the LSFEM does not require any special handling, such as upwinding, staggered grids, artificial dissipation, flux-differencing, etc. Implicit time discretization is used and the scheme is unconditionally stable. By using a matrix-free iterative method, the computational cost and memory requirement for the present scheme is competitive with other approaches. The accuracy of the LSFEM is verified by several benchmark test problems.

1 Introduction

The most widely used numerical method for solving the time-dependent Maxwell equations has been the finite-difference time-domain (FDTD) scheme developed by

*located at Ohio Aerospace Institute, Brook Park, Ohio 44142

Yee [44], and extensively utilized and refined by Taflove et al. [38] and Kunz and Luebbers [21], as well as others (see a recent survey by Shlager and Schneider [35]). In the FDTD, only two Maxwell curl equations are solved by using the explicit time-marching scheme and the central difference approximation. According to Yee's scheme, the electric and magnetic fields are located at different nodes and computed alternatively in time. In other words, the computational mesh for the FDTD has to be structured, and staggered in both time and space to prevent an oscillatory solution from developing as the calculations proceed.

The numerical techniques developed in computational fluid dynamics, based on the conservation laws, have also been applied to solve the time-dependent Maxwell curl equations, including finite-difference (FDTD), finite volume (FVTD) and finite element methods (FEM). All these approaches require some sophisticated treatment, such as upwinding with characteristic-based flux-differencing by Shankar et al. [34] and Shang [31], staggered grids with artificial dissipation by Noack and Anderson [28], or the Taylor-Galerkin method with flux corrected transport by Ambrosiano et al. [2]. It should also be noted that, only for high-speed compressible flow problems, in which shocks occur due to the nonlinearity of the aerodynamics equations, the conservation form is more appropriate, since this formulation often provides a better prediction of the location and strength of the shocks. However, the Maxwell equations in electromagnetics are linear. Except at material interfaces, the solution for such a system of equations is C^0 continuous, i.e., it does not contain sharp, shock-like discontinuities. Therefore, the numerical simulation of problems in computational electromagnetics should not have to resort to the conservation form of equations and the above-mentioned complicated techniques which are closely associated with shock-capturing.

The FEM has become the dominate method for numerical solution of problems in static electromagnetics, eddy currents and waveguides, see, e.g., Silvester and Pelosi [36]. However, application of the node-based FEM to time dependent microwave analysis is rare. Mei et al. [7], Madsen and Ziolkowski [23], Choi et al. [10], Wong et al. [42] and Morgan et al. [25] are among the few papers which can be found in this regard.

In all the above mentioned time-domain approaches, only two curl equations are solved, and the divergence equations are neglected. For frequency-domain computation, such as numerical simulation of waveguide and eddy current problems, it is well known that if the divergence-free constraint is neither forced nor implied, spurious

modes occur and they give particularly high values of $\nabla \cdot \mathbf{B}$, see e.g., Rahman et al. [30], Davies [12], Jin [19] and references therein. However, very few have realized that ignoring the divergence equations in the time-domain computation also leads to spurious solutions. Wu and Jiang [43] first reported some evidence that clearly shows the significant violation of the divergence-free condition near the boundary of scatters in the solutions of the curl equations only. Kangro and Nicolaides [27] also found that time marching solutions of the Maxwell curl equations are contaminated by spurious stationary components and gave a simple technique to remove them. Indeed, it is commonly believed that the divergence-free constrains in the Maxwell equations are redundant, see for example, Kunz and Luebbers ([21], pg. 11). This is usually attributed to the following consideration: taking the divergence of the Faraday and Ampere laws, one finds that these divergence-free conditions are satisfied for all time if they are satisfied initially. However, it is not easy to satisfy them initially by use of the conventional methods, since the inclusion of them will make the system of partial differential equations "overspecified" or "overdetermined", i.e., there will be more equations than unknowns. It is common practice to assume that the initial field intensities are zero throughout the domain, and that the boundary conditions on the surface of the scatterer are correctly given. In this case, the divergence-free condition is significantly violated near the scatterer surface in the first time step of computation. Therefore, there is no guarantee that the computed fields will be divergence-free. However, in many scattered field calculations no attention was directed to the verification of whether the computed field intensities actually satisfied divergence-free conditions. A few exceptions to this are the work by Shang and Gaitonde [32] and by Ambrosiano, et al. [2], in which the values of the divergence of the computed field were numerically examined. It is not difficult to prove that divergence-free conditions are often violated. For example, for two-dimensional TM wave problems, one just needs to show the scattered H_x and H_y contours. Unfortunately, such results are rarely found in computational electromagnetics literature. An exception is the paper by Vinh et al. [40]. In Figs. 2-b and 2-c of that paper, a non-physical solution near the circular cylinder can clearly be observed. Such spurious solutions are a direct result of neglecting the divergence equations, as will be further demonstrated in Section 4.4 of the current report.

It should be mentioned that Assous et al. [3], followed by Sonnendrücker et al. [37], fully realized the importance of the divergence equations in the time-domain Maxwell equations and correctly worked with second-order wave equations. For a special case, they supplemented two divergence equations and an additional boundary condition

to the curl-curl equations. They introduced Lagrange multipliers (which are identical to the "dummy" variables used by the authors for other reason, see [18]) associated to the divergence constrains and reformulated the full Maxwell equations as a constrained variational problem. Then they applied the well-developed mixed Galerkin finite element method in fluid mechanics with the use of non-equal-order elements to solve the problem. This method was one of mathematically solid approaches to deal with the time-domain Maxwell equations.

Boyse and Seidl [5] also realized that node-based methods based on the double curl equations suffers from spurious modes. They pointed out that such a spurious solution is accompanied by ill-conditioned finite element matrices, non-convergent iterative methods, and gross errors in the field calculation. They proposed a hybrid finite element method (HFEM) which combines the node-based FEM and the method of moments (MOM). They used a scalar and vector potential formulation which eliminates spurious solutions. Moreover, the method based on the Helmholtz equation, such as the one used by Bristeau et al. [6] and Dabaghi [11], is also free of spurious modes.

The edge element method [26] is becoming popular for the time domain calculation. The author's opinion regarding edge elements is expressed in [18], and thus will not be repeated here.

Recently, Jiang et al. [15, 18] pointed out that:

1. the principal part, which consists of the first-derivative terms, of the full Maxwell equations in their static, time-harmonic and time-discretized forms, contains two div-curl systems;

2. by introducing a "dummy" variable (this treatment was first proposed by Chang and Gunzburger [9]) which is identically zero, it can be shown that the div-curl system is elliptic and properly determined, i.e., it is not "overdetermined". Consequently the full Maxwell equations are not "overdetermined", and the divergence equations are not redundant;

3. the inclusion of the divergence-free constrains is necessary — to guarantee the uniqueness of the solution in stationary cases, to improve the accuracy of the numerical solution in time-varying cases, and to exclude an infinite degenerate eigenvalue in time-harmonic cases;

4. the satisfaction of the divergence equations can be made easy by using the least-squares method.

The objectives of this paper are (1) to provide an implicit node-based LSFEM for numerical solution of time-dependent full Maxwell equations; (2) to demonstrate that the divergence equations should not be disregarded for time-domain problems; and (3) to supplement our previous paper [18] with time-dependent examples.

The LSFEM is based on the minimization of the L_2 norm of the residuals of first-order systems. As the name implies, the spatial discretization is achieved by using the finite element method. The LSFEM is a universal method for numerical solution of all types of partial differential equations. Further information on the LSFEM can be found in Bochev and Gunzburger [4], Fix and Rose [13], Jiang et al. [14], Jiang and Povinelli [16, 17], Krizek and Neittaanmaki [20] and Lager and Mur [22] among others.

The necessity of implicit schemes for the approximate solution of Maxwell equations have been clearly explained by Adam et al. [1] and Monk [24]. The attraction of implicit time marching schemes is the avoidance of unnecessarily small time steps required by explicit schemes due to the presence of a few small elements in the mesh. The implicit scheme presented in this paper is also inexpensive, since the LSFEM always leads to a symmetric positive definite system of algebraic equations which can be effectively solved by a matrix-free conjugate gradient method. For scattering problems, only a few iterations are needed to advance one time step (more details are provided in Section 3).

In the next section the governing equations and the associated boundary conditions will be presented in detail. The Maxwell equations are naturally of first order and are thus particularly suitable for the LSFEM. The governing equations are first discretized in time using the Crank-Nicolson scheme, then the LSFEM is applied to obtain numerical solutions. The divergence-free conditions are incorporated in the least-squares functional. The discretization procedure is elaborated in Section 3. It will become apparent that the present scheme does not require any special techniques, such as the use of a staggered grid, non-equal-order elements and upwinding, thus, it can be implemented into any existing finite element code in a straight forward manner. The description of the test cases and the numerical results are given in Section 4. Three examples are shown. The first is the polarization by a perfectly conducting circular cylinder at various incident wavelengthes for both transverse-

electric (TE) and transverse-magnetic (TM) waves. The other tests considered are the scattering by a square cylinder and a NACA0012 airfoil. In order to illustrate the importance of the inclusion of divergence-free equations, for the circular cylinder problem, the results of the LSFEM based on the full Maxwell equations are compared with those based on the solution of only the two curl equations, which clearly indicate the occurrence of spurious solutions with large divergence near the scatterers when the divergence-free constraints are neglected. The contours of the spurious solutions observed here also closely resemble those produced by a FD-TD approach [40].

2 Governing Equations

2.1 The Maxwell Equations

In this paper, the time-dependent Maxwell Equations in free space are of interest, which are written as:

$$\nabla \cdot \mathbf{E} = 0, \qquad \text{Gauss' electric law} \tag{1}$$

$$\nabla \cdot \mathbf{H} = 0, \qquad \text{Gauss' magnetic law} \tag{2}$$

$$\varepsilon \mathbf{E}_t - \nabla \times \mathbf{H} = 0, \qquad \text{Ampere's law} \tag{3}$$

$$\mu \mathbf{H}_t + \nabla \times \mathbf{E} = 0, \qquad \text{Faraday's law} \tag{4}$$

where $\mathbf{E}$ and $\mathbf{H}$ are intensities of the electric and magnetic fields respectively; and the physical constants ε and μ are the dielectric permittivity and magnetic permeability of free space.

We note that there are eight equations and six unknown variables in Eqs. (1-4). It has been shown by Jiang et al. [18] that these systems are not overdetermined and that the divergence equations, Eqs. (1) and (2), are not redundant and can be satisfied by the least-squares method.

The objective is to determine the scattered field due to the existence of perfect conducting bodies exposed to plane incident waves in free space. For such cases the field intensity variables are conveniently split into those of the incident field and of the scattered field, such as

$$\mathbf{E} = \mathbf{E}^i + \mathbf{E}^s, \tag{5}$$

$$\text{and} \qquad \mathbf{H} = \mathbf{H}^i + \mathbf{H}^s, \tag{6}$$

where the superscript "i" denotes the incident field; and "s" denotes the scattered field.

By using the above scattered formulation, the incident waves are allowed to propagate in their analytical form. The scattered waves are determined by solving the Maxwell equations with appropriate boundary conditions on the surface of the scatterer and in the far-field.

2.2 Boundary Conditions

On the surface of a perfectly conducting body, the tangential components of the electric intensity and the normal component of the magnetic intensity are both zero, i.e.,

$$\mathbf{n} \times \mathbf{E} = \mathbf{0} \qquad \text{and} \qquad \mathbf{n} \cdot \mathbf{H} = 0, \tag{7}$$

where $\mathbf{n}$ is the outward directed surface normal.

When a scattered field formulation is used, the above becomes:

$$\mathbf{n} \times \mathbf{E}^s = -\mathbf{n} \times \mathbf{E}^i \qquad \text{and} \qquad \mathbf{n} \cdot \mathbf{H}^s = -\mathbf{n} \cdot \mathbf{H}^i. \tag{8}$$

Since the Maxwell equations are now solved in a finite domain, proper far-field boundary conditions have to be applied to ensure that waves will not artificially reflect back and contaminate the near-field solution. Here we adopt the following absorbing boundary condition:

$$\frac{1}{c}\frac{\partial \phi}{\partial t} + \frac{\partial \phi}{\partial n} = 0, \tag{9}$$

where $\mathbf{n}$ is the outward directed normal of the far-field boundary, ϕ is any component of $\mathbf{E}^s$ and $\mathbf{H}^s$, and $c = 1/\sqrt{\varepsilon\mu}$ is the wave velocity. This absorbing boundary condition can be easily implemented in the current version of our general-purpose LSFEM code.

It should be noted that in electromagnetic scattering problems normally only the solution in the near-field is of interest. Indeed the radar cross section (RCS) calculation requires only the field intensities on the surface of the scatterer (see Section

4). Because the absorbing boundary condition given in Eq. (9) is only an approximation of the true absorbing boundary condition, the computational domain needs to be larger than those using higher-order absorbing conditions. However, at the far-field it is only required that the waves propagate out and do not reflect back to contaminate the near field solutions, the accuracy of the solution there is of no interest. For this reason it is most efficient to refine the mesh locally near the surface of the scatterer and to use a coarse mesh in the far-field. The use of such non-uniform grids is easily accommodated in the present scheme since the calculation is carried out totally on an unstructured mesh. Due to the use of a non-uniform grid and large elements near the far-field boundary, the elements placed in the part of the computational domain far from the scatterer surface represent only a small proportion of the total element number. Thus the present approach still provides a very good approximation of the field variables while maintaining efficiency. We will later show in Section 4 that satisfactory results are obtained using such non-uniform meshes. We remark that this refinement strategy is not new. Ambrosiano et al. [2] and Vinh et al. [40] have used grids with large size variation and obtained satisfactory RCS. We also want to emphasize that this concept of local refinement differs from that based on a uniform distribution of error, which is widely used in solid mechanics and other fields.

2.3 Transverse-Magnetic (TM) and Transverse-Electric (TE) Forms in Two Dimensions

If the electromagnetic fields are two-dimensional, all derivatives with respect to the third dimension become zero, and some components of the field intensity variables vanish. There exist two sets of distinct modes, that is, the Transverse-Magnetic (TM) mode and Transverse-Electric (TE) mode.

For TM waves, we have

$$H_z = 0, E_x = 0, E_y = 0. \tag{10}$$

The governing equations, Eqs. (1-4), become:

$$\varepsilon \frac{\partial E_z}{\partial t} - \frac{\partial H_y}{\partial x} + \frac{\partial H_x}{\partial y} = 0, \tag{11}$$

$$\mu \frac{\partial H_x}{\partial t} + \frac{\partial E_z}{\partial y} = 0, \tag{12}$$

$$\mu\frac{\partial H_y}{\partial t} - \frac{\partial E_z}{\partial x} = 0, \tag{13}$$

$$\frac{\partial H_x}{\partial x} + \frac{\partial H_y}{\partial y} = 0. \tag{14}$$

Whereas for TE waves,

$$E_z = 0, H_x = 0, H_y = 0, \tag{15}$$

and the governing equations are simplified as:

$$\mu\frac{\partial H_z}{\partial t} + \frac{\partial E_y}{\partial x} - \frac{\partial E_x}{\partial y} = 0, \tag{16}$$

$$\varepsilon\frac{\partial E_x}{\partial t} - \frac{\partial H_z}{\partial y} = 0, \tag{17}$$

$$\varepsilon\frac{\partial E_y}{\partial t} + \frac{\partial H_z}{\partial x} = 0, \tag{18}$$

$$\frac{\partial E_x}{\partial x} + \frac{\partial E_y}{\partial y} = 0. \tag{19}$$

3 Discretization of the Governing Equations

Equations (1-4) are first discretized in time, using the Crank-Nicolson scheme. This scheme provides second order accuracy in time and is known to be nondissipative when used in conjunction with central space differences. Although this scheme is unconditionally stable and thus poses no limitation on the time step, the dispersive error becomes large if very large time step is used. Thus, care should be taken when choosing the size of the time step. To maintain the accuracy in the time domain, we typically use a time step corresponding to a CFL number between 1 and 2 at the smallest element.

After applying time discretization to Eqs. (1-4), we have,

$$\nabla \cdot \mathbf{E}^{n+1} = 0 \tag{20}$$

$$\nabla \cdot \mathbf{H}^{n+1} = 0 \tag{21}$$

$$\varepsilon\frac{\mathbf{E}^{n+1} - \mathbf{E}^n}{\Delta t} - \frac{1}{2}\nabla \times \left(\mathbf{H}^n + \mathbf{H}^{n+1}\right) = 0 \tag{22}$$

$$\mu\frac{\mathbf{H}^{n+1} - \mathbf{H}^n}{\Delta t} + \frac{1}{2}\nabla \times \left(\mathbf{E}^n + \mathbf{E}^{n+1}\right) = 0 \tag{23}$$

where the superscript n denotes the n^{th} time step.

Equations (20-23) can be rewritten into a compact matrix form as:

$$\mathbf{A}\mathbf{u} + \mathbf{A}_1\frac{\partial \mathbf{u}}{\partial x} + \mathbf{A}_2\frac{\partial \mathbf{u}}{\partial y} + \mathbf{A}_3\frac{\partial \mathbf{u}}{\partial z} = \mathbf{f} \tag{24}$$

where

$$\mathbf{u} = \begin{bmatrix} E_x^{n+1} \\ E_y^{n+1} \\ E_z^{n+1} \\ H_x^{n+1} \\ H_y^{n+1} \\ H_z^{n+1} \end{bmatrix}, \quad \mathbf{f} = \begin{bmatrix} 0 \\ 0 \\ \frac{1}{2}\left(\frac{\partial H_z^n}{\partial y} - \frac{\partial H_y^n}{\partial z}\right) + \varepsilon\frac{E_x^n}{\Delta t} \\ \frac{1}{2}\left(\frac{\partial H_x^n}{\partial z} - \frac{\partial H_z^n}{\partial x}\right) + \varepsilon\frac{E_y^n}{\Delta t} \\ \frac{1}{2}\left(\frac{\partial H_y^n}{\partial x} - \frac{\partial H_x^n}{\partial y}\right) + \varepsilon\frac{E_z^n}{\Delta t} \\ \frac{1}{2}\left(\frac{\partial E_z^n}{\partial y} - \frac{\partial E_y^n}{\partial z}\right) + \mu\frac{H_x^n}{\Delta t} \\ \frac{1}{2}\left(\frac{\partial E_x^n}{\partial z} - \frac{\partial E_z^n}{\partial x}\right) + \mu\frac{H_y^n}{\Delta t} \\ \frac{1}{2}\left(\frac{\partial E_y^n}{\partial x} - \frac{\partial E_x^n}{\partial y}\right) + \mu\frac{H_z^n}{\Delta t} \end{bmatrix},$$

$$\mathbf{A} = \begin{bmatrix} 0 & 0 & 0 & 0 & 0 & 0 \\ 0 & 0 & 0 & 0 & 0 & 0 \\ \varepsilon\frac{1}{\Delta t} & 0 & 0 & 0 & 0 & 0 \\ 0 & \varepsilon\frac{1}{\Delta t} & 0 & 0 & 0 & 0 \\ 0 & 0 & \varepsilon\frac{1}{\Delta t} & 0 & 0 & 0 \\ 0 & 0 & 0 & \mu\frac{1}{\Delta t} & 0 & 0 \\ 0 & 0 & 0 & 0 & \mu\frac{1}{\Delta t} & 0 \\ 0 & 0 & 0 & 0 & 0 & \mu\frac{1}{\Delta t} \end{bmatrix}, \quad \mathbf{A}_1 = \begin{bmatrix} 1 & 0 & 0 & 0 & 0 & 0 \\ 0 & 0 & 0 & 1 & 0 & 0 \\ 0 & 0 & 0 & 0 & 0 & 0 \\ 0 & 0 & 0 & 0 & 0 & \frac{1}{2} \\ 0 & 0 & 0 & 0 & -\frac{1}{2} & 0 \\ 0 & 0 & 0 & 0 & 0 & 0 \\ 0 & 0 & -\frac{1}{2} & 0 & 0 & 0 \\ 0 & \frac{1}{2} & 0 & 0 & 0 & 0 \end{bmatrix},$$

$$\mathbf{A}_2 = \begin{bmatrix} 0 & 1 & 0 & 0 & 0 & 0 \\ 0 & 0 & 0 & 0 & 1 & 0 \\ 0 & 0 & 0 & 0 & 0 & -\frac{1}{2} \\ 0 & 0 & 0 & 0 & 0 & 0 \\ 0 & 0 & 0 & \frac{1}{2} & 0 & 0 \\ 0 & 0 & \frac{1}{2} & 0 & 0 & 0 \\ 0 & 0 & 0 & 0 & 0 & 0 \\ -\frac{1}{2} & 0 & 0 & 0 & 0 & 0 \end{bmatrix}, \quad \mathbf{A}_3 = \begin{bmatrix} 0 & 0 & 1 & 0 & 0 & 0 \\ 0 & 0 & 0 & 0 & 0 & 1 \\ 0 & 0 & 0 & 0 & \frac{1}{2} & 0 \\ 0 & 0 & 0 & -\frac{1}{2} & 0 & 0 \\ 0 & 0 & 0 & 0 & 0 & 0 \\ 0 & -\frac{1}{2} & 0 & 0 & 0 & 0 \\ \frac{1}{2} & 0 & 0 & 0 & 0 & 0 \\ 0 & 0 & 0 & 0 & 0 & 0 \end{bmatrix} \tag{25}$$

The two-dimensional TM and TE cases are presented in the same form, with the corresponding zero terms dropped.

Eq. (24) is then discretized in space following the standard LSFEM procedure [16]. This results in a set of algebraic equations which can be written as:

$$\mathbf{K}\mathbf{U} = \mathbf{F} \tag{26}$$

In the above, it is implied that the following standard finite element approximation to the unknown variables $\mathbf{u}$ has already been introduced, i.e.,

$$\mathbf{u} \approx \hat{\mathbf{u}} \equiv \mathbf{NU} \tag{27}$$

where $\hat{\mathbf{u}}$ is the finite element approximation to $\mathbf{u}$ and $\mathbf{U}$ are the nodal values; $\mathbf{N}$ are the finite element shape functions.

The matrix $\mathbf{K}$ in Eq. (26) is defined by the matrices $\mathbf{A}$ and $\mathbf{A}_i$ in Eq. (24) and shape functions $\mathbf{N}$ in Eq. (27) as:

$$\mathbf{K} = \int_{\Omega} [\mathbf{L}(\mathbf{N})]^T \mathbf{L}(\mathbf{N}) d\Omega \tag{28}$$

in which

$$\mathbf{L}(\mathbf{N}) = \mathbf{AN} + \sum_{i=1,3} \mathbf{A}_i \mathbf{N}_{,i}$$

and $[\mathbf{L}(\mathbf{N})]^T$ denotes the transpose of the matrix $\mathbf{L}(\mathbf{N})$; Ω is the domain of the problem.

The right hand side vector in Eq. (26) is defined by:

$$\mathbf{F} = \int_{\Omega} [\mathbf{L}(\mathbf{N})]^T \mathbf{f} d\Omega \tag{29}$$

where $\mathbf{f}$ is the right hand side of equation (24).

At this stage it becomes clear that once the governing equation set is written in the form of the standard first-order system, i.e., Eq. (24), the LSFEM can be easily incorporated into any existing finite element code in a straight forward manner. One advantage of using the LSFEM is that the computer code can be constructed in a general-purpose setting for the system of equations in Eq. (24) in such a way that the only required programming for application to a new problem is to write a subroutine to supply the matrices $\mathbf{A}$, $\mathbf{A}_i$ and $\mathbf{f}$, therefore the tedious work is reduced to a minimum.

We have used a Jacobi-preconditioned conjugate gradient method to solve the resulting algebraic equation system, Eq. (26). By using this method, the iterations can be performed in such a matrix-free manner that there is no need to assemble the global matrix $\mathbf{K}$ or to form the element matrices [8]. This has greatly reduced the requirement for computer memory. We have found that five conjugate gradient iterations are enough to guarantee the accuracy of the solution in our calculations.

The use of such a small number of iterations can be attributed to the fact that when the time step is small (corresponding to a CFL number between 1 and 2), the solution in the previous time step serves as a very good initial guess for the next step, thus the conjugate gradient method needs fewer iterations than the case when a larger time step is used. Therefore, although the current method takes the form of an implicit method, its computational speed is competitive with an explicit method.

4 Numerical Examples

Several test cases of the scattering of a plane incident wave by perfect conducting bodies will be presented. Since the purpose of this paper is to validate the present scheme and show the importance of the divergence equations, the numerical examples will be confined to two dimensional problems. We believe these cases sufficiently demonstrate our view points. We have successfully carried out preliminary calculations for three dimensional problems and have recently reported these results [43].

The incident sinusoidal wave is given by:

$$E^{z,i} = E_0 \sin k(x\cos\alpha + y\sin\alpha - ct),$$

$$H^{x,i} = \frac{E^{z,i}\sin\alpha}{\mu c},$$

$$H^{y,i} = -\frac{E^{z,i}\cos\alpha}{\mu c}$$

for TM case; and

$$H^{z,i} = H_0 \sin k(x\cos\alpha + y\sin\alpha - ct),$$

$$E^{x,i} = -\frac{H^{z,i}\sin\alpha}{\varepsilon c},$$

$$E^{y,i} = \frac{H^{z,i}\cos\alpha}{\varepsilon c}$$

for TE case. Here c is the wave velocity defined in Section 2; k is the wave number; α is the angle of incidence.

The numerical results will be presented in terms of the surface current (for TM case only) and radar cross section (RCS). The calculation of these requires the field

variables in the frequency domain, thus a Fourier transform is performed to transfer the field variables from the time domain to the frequency domain.

The surface current J_s for TM case is defined as

$$J_s = \frac{|\mathbf{n} \times \mathbf{H}_t|}{|\mathbf{H}_i|},$$

where $\mathbf{H}_i$ and $\mathbf{H}_t$ are the incident and total magnetic fields in the frequency domain, respectively.

The radar cross section (RCS) for TM wave, S_{TM}, is defined as:

$$S_{TM}(\theta) = \lim_{\rho \to \infty} 2\pi\rho \left| \frac{E_z^s(\rho, \theta)}{E_z^i} \right|^2, \tag{30}$$

where E_z^s and E_z^i are the scattered and incident electric fields, respectively, in the frequency domain; ρ is the distance from the center of the scattering object; and θ is the angle of observation. Note that the calculation of S_{TM} from the above expression requires knowledge of E_z^s at an infinite distance from the scatterer. This is not available since the Maxwell equations are solved in a finite domain. However, the far-field solution can be obtained from the distribution on a near-field surface (the most convenient one being the surface of the scatterer) by a transformation using Green's function, as described by Shankar et al. [33]. This transformation is adopted in this paper to obtain the RCS.

For TE wave, the RCS S_{TE} is defined as:

$$S_{TE}(\theta) = \lim_{\rho \to \infty} 2\pi\rho \left| \frac{H_z^s(\rho, \theta)}{H_z^i} \right|^2. \tag{31}$$

The calculation of S_{TE} follows the same procedure as TM cases.

Bilinear quadrilateral elements for all variables are used in all cases. The meshes are generated using the unstructured mesh generator developed by Zhu et al. [45], based on the advancing front technique of Peraire et al. [29].

4.1 Circular Cylinder

The first example deals with a scattering field due to a circular perfect conducting circular cylinder. Both TM and TE cases at various wavelengthes are considered.

The definition of the problem is given in Fig. 1. This problem allows an analytical solution in a series form, see, e.g., Umashankar and Taflove [39]. Due to the symmetry of this problem, only a half of the domain is used. The computational mesh consists of 2538 nodes and 2435 elements, with 142 divisions on the cylinder surface (Fig. 2). Figs. 3-4 show the calculated RCS. Fig. 5 shows the calculated surface current for TM cases and compares the LSFEM results with the analytical solutions which are calculated from the series form presented in [39] using *Mathematica* [41]. The instantaneous distributions of the scattered field variables are shown in Figs. 6-7.

4.2 Square Cylinder

The second example concerns scattering by a square cylinder defined in Fig. 8. The TM case with $ka = 1$ is considered. The computational mesh consists of 2749 bilinear quadrilateral elements with 2874 nodes (Fig. 9). Fig. 10 shows the surface current distribution. Comparison is made with the results by Shankar et al. [34] and that obtained by Umashankar and Taflove [39] using the method of moments (MOM). The instantaneous E_z contours are shown in Fig. 11.

4.3 NACA0012 Airfoil

Preliminary results are presented here for two cases of scattered TM wave due to a NACA0012 airfoil (Fig. 12). The angles of incidence are 0 and 90 degrees; and the values of ka are 10 and 10π, respectively. Fig. 13 shows the computational mesh, which consists of 1782 bilinear elements and 1912 nodes. There are 156 divisions on the surface of the airfoil. Fig. 14 shows the contours of E_Z for the 0 degree incidence case. Figs. 15 and 16 show the computed RCS. The case of 90 degree incidence is compared with those by Shankar et al. [34] and Vinh et al. [40]. Generally, fair agreement is observed. Note that we have used a very coarse mesh and a very small domain.

4.4 Importance of the Divergence Equations

To illustrate the influence of the inclusion of divergence equations, we present here a comparison of two groups of numerical solutions, both obtained by using the LSFEM: the first group is obtained by solving the full Maxwell equations, while the second group is obtained by solving solely the two curl equations. Here the case of TM waves scattered by a circular cylinder is considered. The values of ka used here are $ka = 1$ and $ka = 10$. Fig. 17 shows a comparison of the contours of the field variables for $ka = 1$ between the group 1 and the group 2. It is clearly revealed that without enforcing the divergence condition significant spurious patterns exist for H_x and H_y near the surface. Further calculation shows that indeed the group 2 solution possesses very large divergence of $\mathbf{H}$ in the vicinity of the scatterer surface. The absolute value of $\nabla \cdot \mathbf{H}$ reaches its maximum of 21.28 in an element adjacent to the surface. On the other hand, the maximum value of $\nabla \cdot \mathbf{H}$ for the group 1 is 0.054, which occurs near the outer boundary. The divergence-free condition for $\mathbf{E}$ is automatically satisfied, therefore almost identical E_z distributions are obtained with the two formulations. Fig. 18 shows the field variables for $ka = 10$. Again a non-physical solution is found for the group 2 solution near the surface. These non-physical patterns are similar to those in Figs. 2-b and 2-c of [40].

We should remark here that although group 1 and group 2 solutions differ significantly, very little difference was observed in the RCS calculations based on the two solutions. This is due to the fact that the erroneous part of the solution is static, and the static field does not radiate. Definitely, the erroneous solutions of the field intensities caused by the neglect of the divergence conditions cannot be accepted, for example, in plasma computations and in the computation of impedance in digital circuits and electronic packaging.

5 Concluding Remarks

A node-based least-squares finite element method has been presented for the time-dependent Maxwell equations for scattering problems. Divergence-free conditions have been included in the least-squares functional thus eliminating the existence of spurious modes. This technique is also expected to be useful for the solution of Vlasov-Maxwell equations in plasma physics and the simulation of magnetohydrodynamics (MHD), and for the modeling of microwave integrated circuit components.

The accuracy of the scheme has been verified by various benchmark tests. The computation is carried out on a totally unstructured mesh which has a rather large distribution of grid sizes. This provides a great amount of flexibility in dealing with complex geometries. The scheme is implicit and unconditionally stable, therefore, it offers significant advantages in handling electromagnetic problems whose element size varies several orders of magnitude across the problem domain. In those situations the time step will no longer be determined by the smallest size as in explicit schemes. Although this method is implicit, due to the use of the matrix-free conjugate gradient method, there is no matrix inversion, and thus the computational cost and memory requirements are competitive with explicit approaches.

In this report, we have demonstrated that the omission of the divergence equations in the numerical procedure produces non-physical solutions for scattered field problems, we have therefore shown that the common belief that the divergence equations are redundant is a serious misconception. The possibility of producing spurious solutions from time-domain methods should not be overlooked, even though it does not affect the computed RCS.

References

[1] J. Adam, A. Serveniere, J. Nédélec and P. Raviart, Study of an implicit scheme for integrating Maxwell's equations, Comp. Meth. Appl. Mech. Engng., **22**, 327-346 (1994).

[2] J. J. Ambrosiano, S. T. Brandon and R. Lohner, Electromagnetics via the Taylor-Galerkin finite element method on unstructured grids, J. Comp. Phys., **110**, 310-319 (1994).

[3] F. Assous, P. Degond, E. Heintze, P.A. Raviart and J. Seger, On a finite-element method for solving the three-dimensional Maxwell equations, J. Comp. Phys., **109**, 222-237 (1993).

[4] P. B. Bochev and M. D. Gunzburger, Accuracy of least-squares methods for the Navier-Stokes equations, Comput. and Fluids, **22**, 549-563 (1993).

[5] W. E. Boyse and A. A. Seidl, A hybrid finite element method for 3-D scattering using nodal and edge elements, IEEE Trans. Antennas and Popagat., **42**, 1436-1442 (1994).

[6] M. -O. Bristeau, R. Glowinski and J. Periaux, Wave scattering at high wave numbers using exact controllability and finite element methods, IEEE Trans. Magnetics, **31** 1530-1533 (1995).

[7] A. C. Cangellaris, C. -C. Lin and K. K. Mei, Point-matched time domain finite element methods for electromagnetic radiation and scattering, IEEE Trans. Antennas and Popagat., **35**, 1160-1173 (1987).

[8] G. F. Carey and B. N. Jiang, Element-by-element linear and non-linear solution methods, Commun. Appl. Num. Methods, **2**, 145-153 (1986).

[9] C. L. Chang and M. D. Gunzburger, A finite element method for first order elliptic systems in three dimensions, Appl. Math. and Comput., **23**, 171-184 (1987).

[10] K. Choi, K. A. Connor, L. F. Libelo and S. Y. hahn, Time domain finite element analysis of high power microwave aperture antennas, IEEE Trans. Magnetics, **31**, 1622-1625 (1995).

[11] F. E. Dabaghi, Finite element solutions and full second order absorbing boundary conditions for 2D unsteady Maxwell equations, in *Second International Conference on Mathematical and Numerical Aspects of Wave Propagation*, edited by I. Stakgold et al., (SIAM, Philadelphia, 1993), 207-216.

[12] J. B. Davies, Finite element analysis of waveguides and cavities — a review, IEEE Trans. Magnetics, **29**, 1578-1583 (1993).

[13] G. J. Fix and M. E. Rose, A comparative study of finite element and finite difference methods for Cauchy-Riemann type equations, SIAM J. Numer. Anal., **22**, 250-261 (1985).

[14] B. N. Jiang, T. L. Lin and L. A. Povinelli, Large-scale computation of incompressible viscous flow by least-squares finite element method, Comp. Meth. Appl. Mech. Engng., **114**, 213-231 (1994).

[15] B. N. Jiang, C. Y. Loh and L. A. Povinelli, Theoretical study of the incompressible navier-stokes equations by the least-squares method, NASA TM 106535, ICOMP-94-04.

[16] B. N. Jiang and L. A. Povinelli, Least-squares finite element method for fluid dynamics, Comp. Meth. Appl. Mech. Engng., **81**, 13-37 (1990).

[17] B. N. Jiang and L. A. Povinelli, Optimal least squares finite element method for elliptic problems, Comp. Meth. Appl. Mech. Engng., **102**, 199-212 (1993).

[18] B. N. Jiang, J. Wu, and L. A. Povinelli, The origin of spurious solutions in computational electromanetics, J. Comp. Phys., **125**, 104-123 (1996), see also NASA TM 106921, ICOMP-95-8.

[19] J. M. Jin, *The Finite Element Method in Electro-Magnetics*, (John Wiley and Sons, New York, 1993).

[20] M. Krizek and P. Neittaanmäki, *Finite Element Approximation of Variational Problems and Applications* (Pitman Scientific and Technical, Hawlow, England, 1990).

[21] K. S. Kunz and R. J. Luebbers, *The Finite Difference Time Domain Method for Electro-Magnetics* (CRC Press, Boca Raton, 1993).

[22] I. E. Lager and G. Mur, The finite element modeling of static and stationary electric and magnetic field, IEEE Transactions on Magnetics, Vol. 32, no.3 631-634 (1996).

[23] N. K. Madsen and R. W. Ziolkowski, Numerical solution of Maxwell's equations in the time domain using irregular nonorthogonal grids, Wave Motion, **10**, 583-596 (1988).

[24] P. Monk, Finite element time domain methods for Maxwell's equations, in *Second International Conference on Mathematical and Numerical Aspects of Wave Propagation*, edited by I. Stakgold et al., (SIAM, Philadelphia, 1993), 380-389.

[25] K. Morgan, O. Hassan and J. Peraire, Time domain unstructured grid approach to the simulation of electromagnetic scattering in piecewise homogeneous media, Comp. Meth. Appl. Mech. Engng., **134**, 17-36 (1996).

[26] J. Nedelec, A new family of mixed finite elements in $\mathbf{R}^3$, Numer. math. **50**, 57-81 (1986).

[27] U. Kangro and R. Nicolaides, Spurious fields in time domain computations of scattering problems, NASA Contractor Report 198223, ICASE Report 95-69.

[28] R. W. Noack and D. A. Anderson, Time-domain solutions of Maxwell's equations using a finite-volume formulations, AIAA Paper 92-0451.

[29] J. Peraire, M. Vahadati, K. Morgan and O. C. Zienkiewicz, Adaptive remeshing for compressible flow computations, J. Comp. Phys., **72**, 449-466 (1987).

[30] B. M. A. Rahman, F. A. Fernandez and J. B. Davies, Review of finite element methods for microwave and optical waveguides, Proc. of the IEEE, **79**, 1442-1448 (1991).

[31] J. S. Shang, Characteristic-based algorithms for solving the Maxwell equations in the time domain, IEEE Antennas and Propagation Magazine, **37**, 15-25 (1995).

[32] J. S. Shang and D. Gaitonde, Scattered electromagnetic field of a reentry vehicle, AIAA 94-0231.

[33] V. Shankar, W. F. Hall, A. Mohammadian and C. Rowell, Computational electromagnetics (CEM), development of a finite-volume, time-domain solver for Maxwell's equations: A final report for NASA/NADC contract N62269-90-C-0257 (1993).

[34] V. Shankar, F. H. William and A. H. Mohammadian, A time-domain differential solver for electromagnetic scattering problems, Proc. of the IEEE, **77**, 709-721 (1989).

[35] K. L. Shlager and J. B. Schneider, A selective survey of the finite-difference time-domain literature, IEEE Antennas and Propagation Magazine, **37**, 39-56 (1995).

[36] P. P. Silvester and G. Pelosi, *Finite Element for Wave Electromagnetics* (IEEE Press, New York, 1994).

[37] E. Sonnendrückern, J. J. Ambrosiano and S. T. Brandon, A finite element formulation of the Darwin PIC model for use on unstructured grids, J. Comp. Phys., **121**, 281-297 (1995).

[38] A. Taflove and K. R. Umashankar, Review of FD-TD numerical modeling of electromagnetic wave scattering and radar cross section, Proceedings of IEEE, **77**, 682-699 (1989).

[39] A. Taflove, *Computational Electrodynamics*, the finite-difference time-domain method (Artech House, Boston, Massachusetts, 1995).

[40] H. Vinh, H. A. Dwyer and C. P. van Dam, Finite-difference algorithms for the time-domain Maxwell's equations — a numerical approach to RCS analysis, AIAA Paper 92-2989.

[41] S. Wolfram, *Mathematica: A System for Doing Mathematics by Computer* (Addison-Wesley, 1988).

[42] M. F. Wong, O. Picon and V. F. Hanna, A finite element method based on whitney forms to solve Maxwell equations in the time domain, IEEE Trans. Magnetics, **31**, 1618-1621 (1995).

[43] J. Wu and B. N. Jiang, A Least-Squares Finite Element Method for electromagnetic scattering problems, in Proceedings of the Third US National Congress on Computational Mechanics (USNCCM III), Texas, Dalas, edited by J. N. Reddy, et al., 1995.

[44] K. S. Yee, Numerical solution of initial boundary value problems involving Maxwell's equations in isotropic media, IEEE Trans. Antennas Propagat., **AP-14**, 302-307 (1966).

[45] J. Z. Zhu, O. C. Zienkiewicz, E. Hinton and J. Wu, A new approach to the development of automatic quadrilateral mesh generation, Int. J. Num. Meth. Engng., **32**, 849-866 (1991).

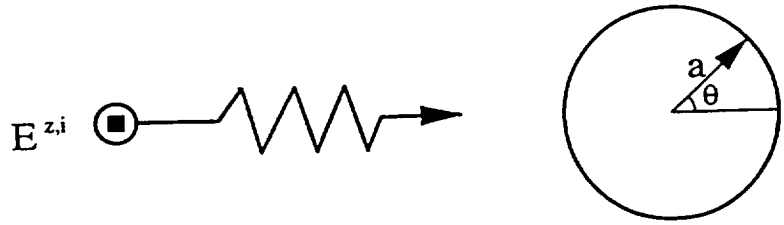

Figure 1 Scattering by a circular cylinder: problem definition

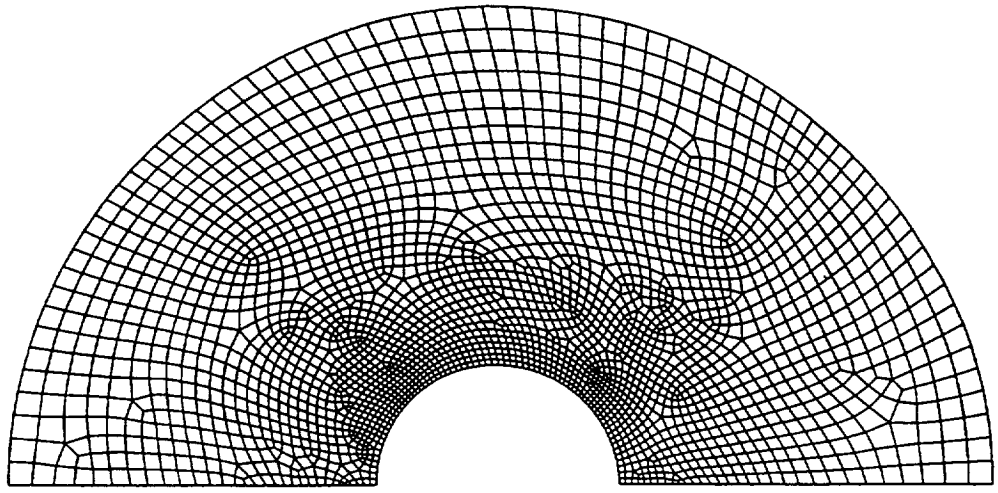

Figure 2 Scattering by a circular cylinder: finite element mesh

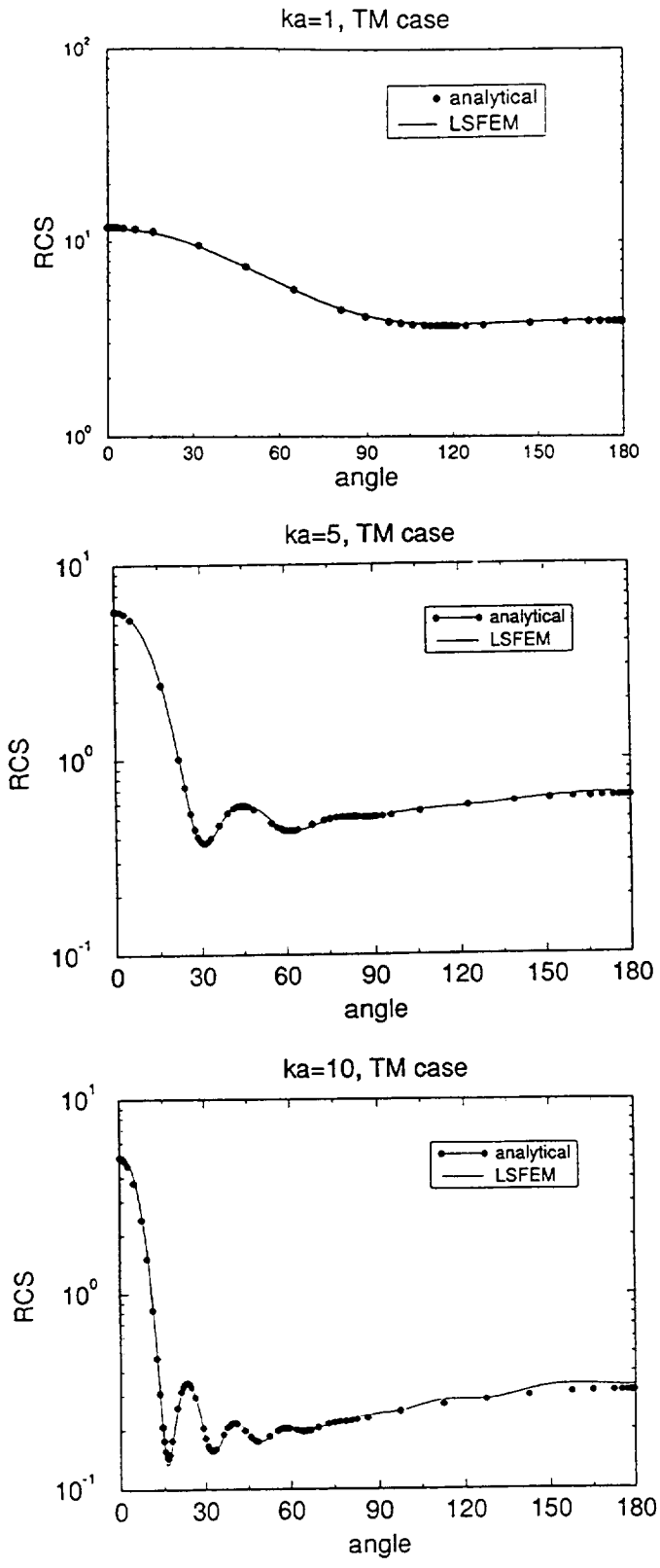

Figure 3 RCS for the circular cylinder (TM mode)

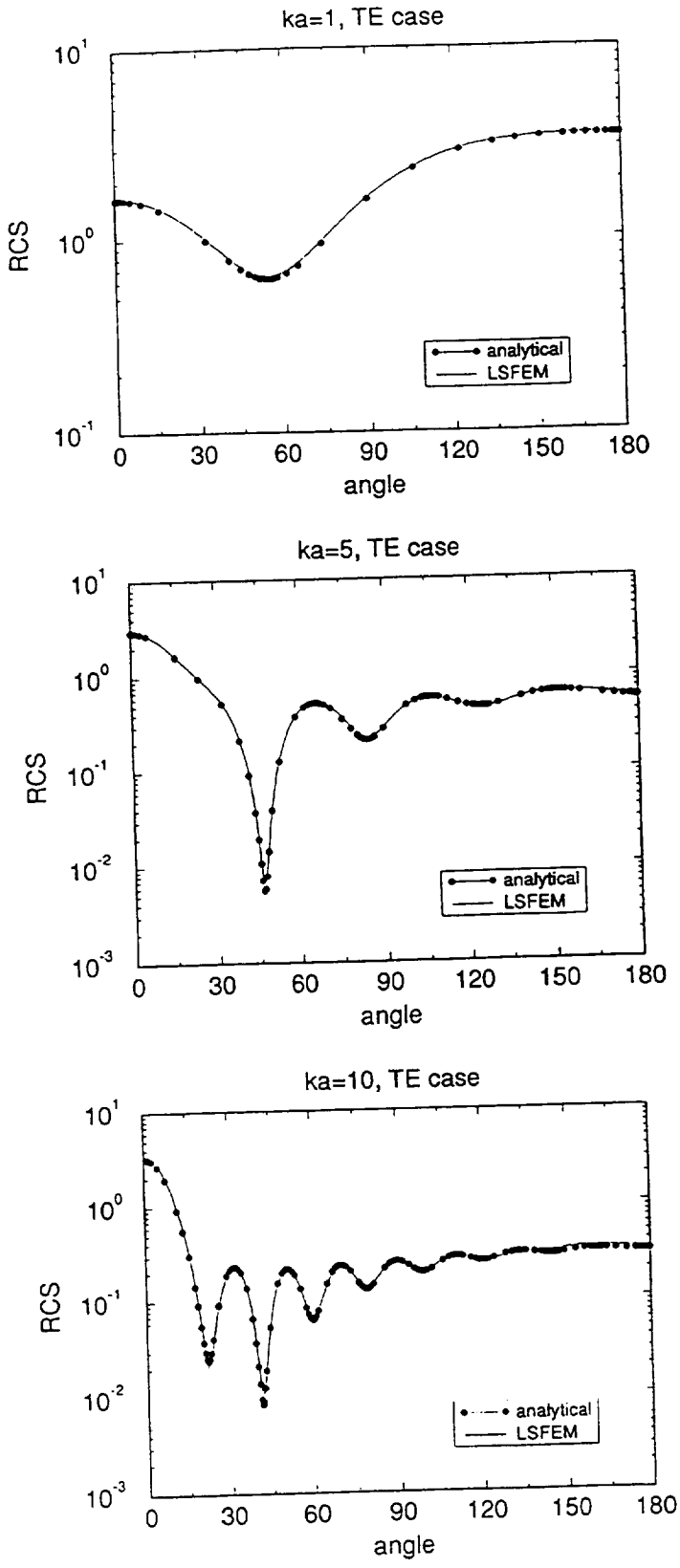

Figure 4 RCS for the circular cylinder (TE mode)

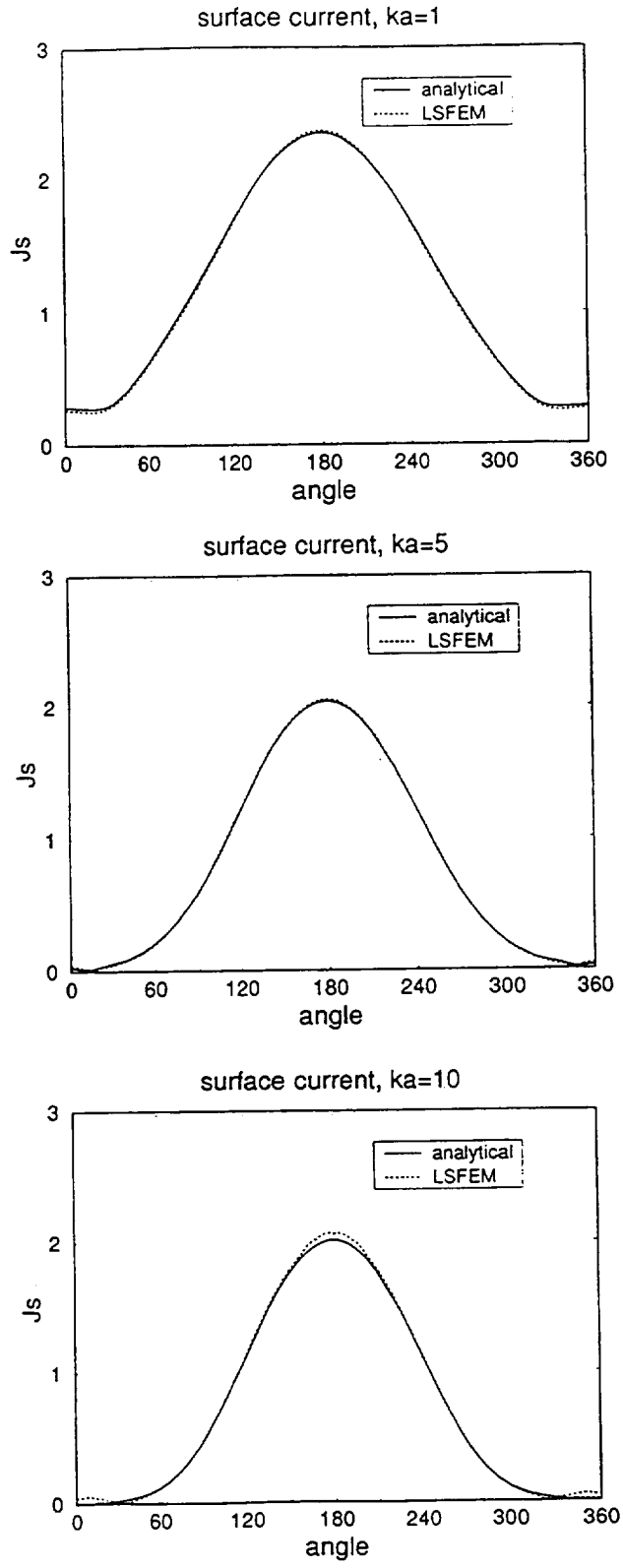

Figure 5 Normalized surface current for the circular cylinder

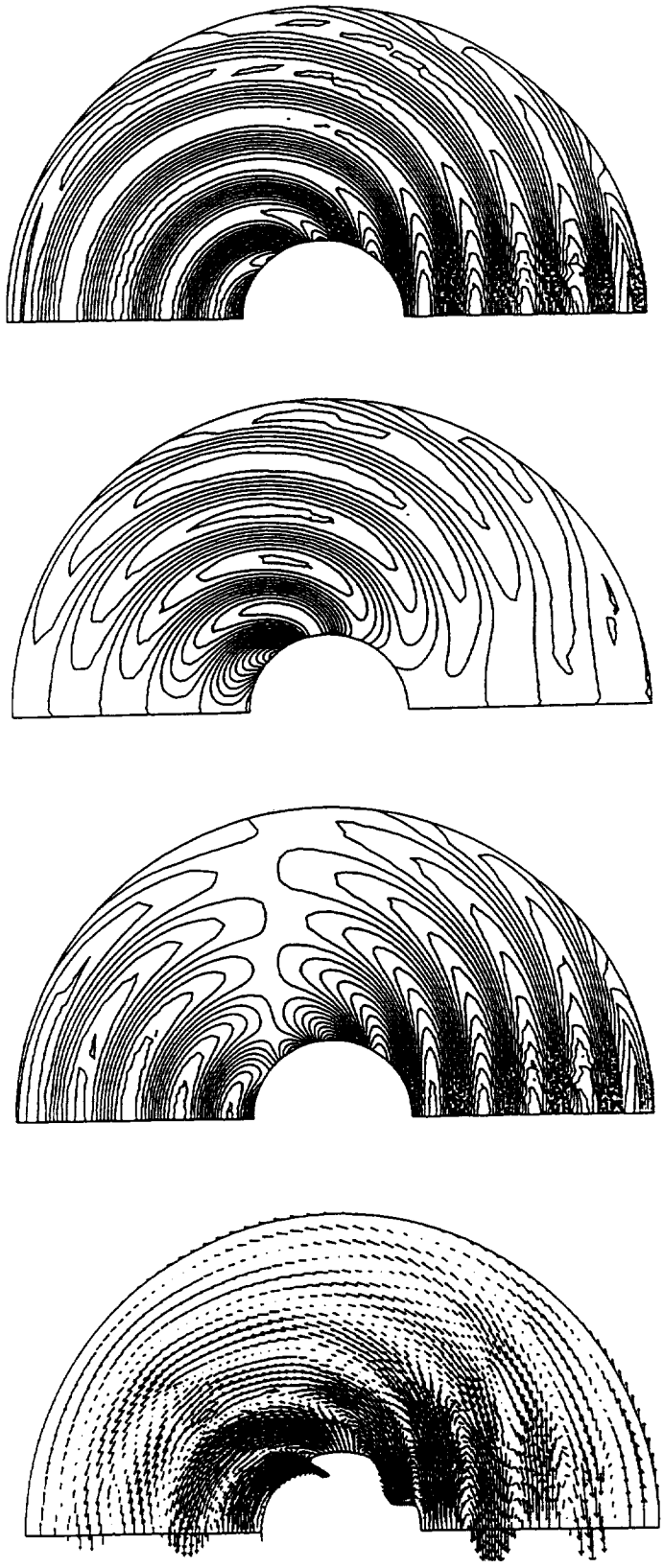

Figure 6 Scattered fields for the circular cylinder
(E_z, H_x, H_y contours and H vectors, TM mode, $ka = 5$)

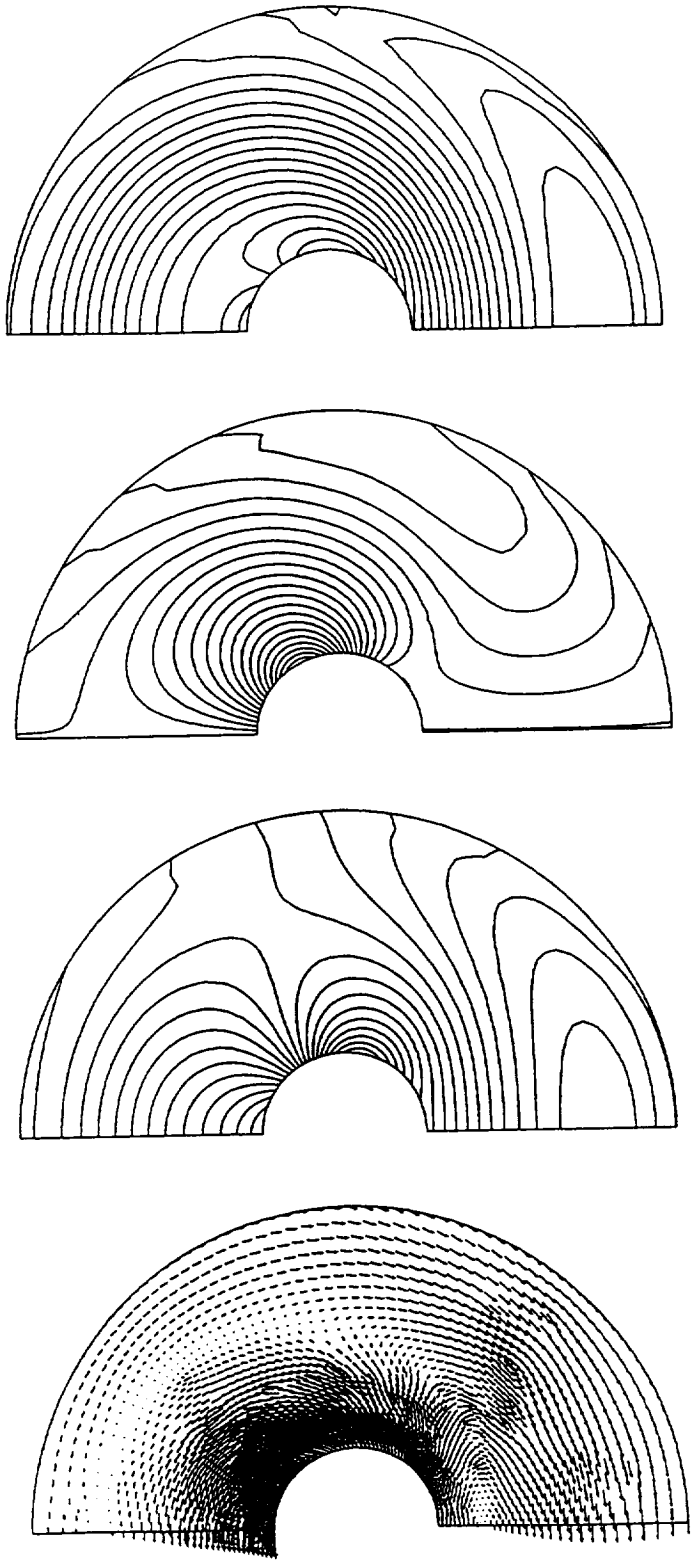

Figure 7 Scattered fields for the circular cylinder
(E_z, H_x, H_y contours and **H** vectors, TM mode, $ka = 1$)

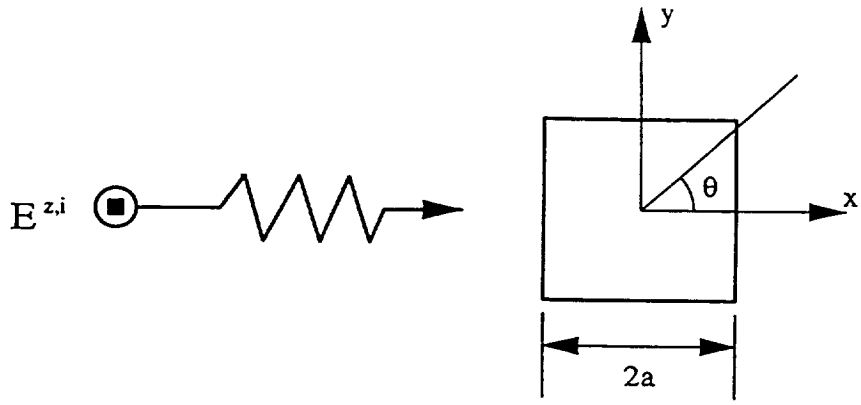

Figure 8 Scattering by a square cylinder: problem definition

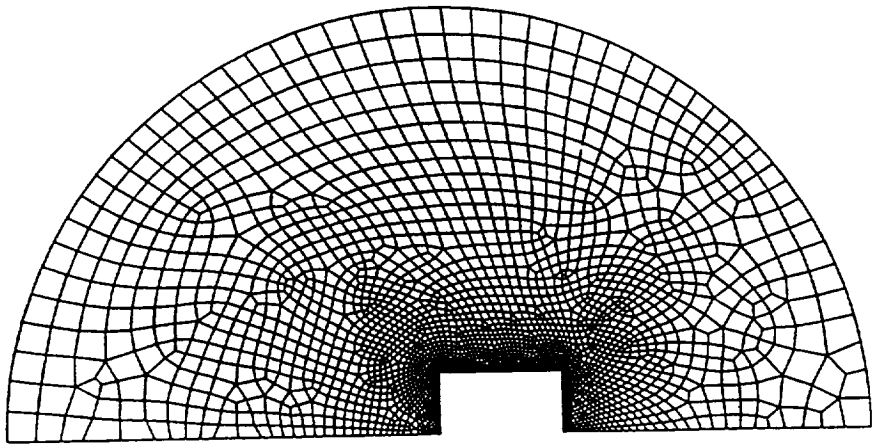

Figure 9 Scattering by a square cylinder: finite element mesh

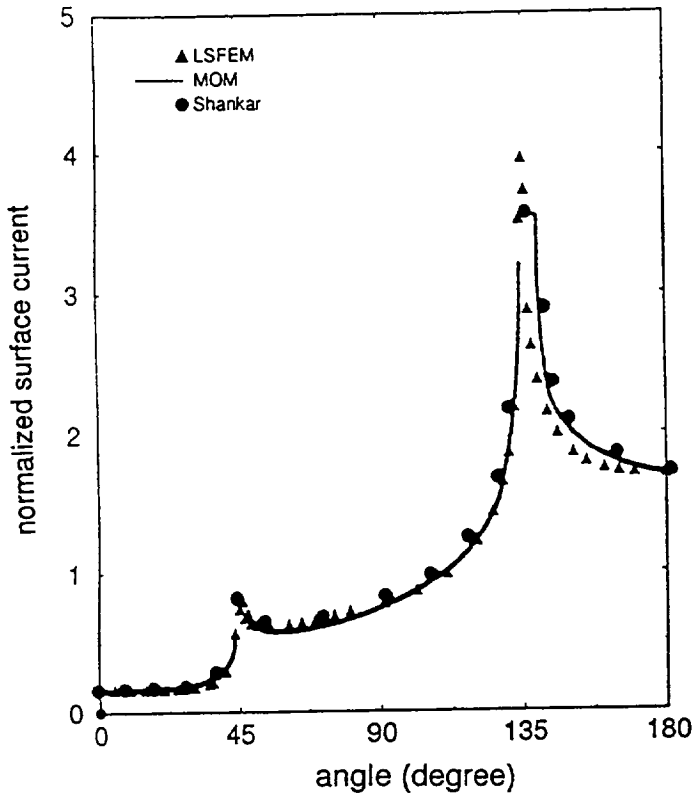

Figure 10 Normalized surface current for the square cylinder

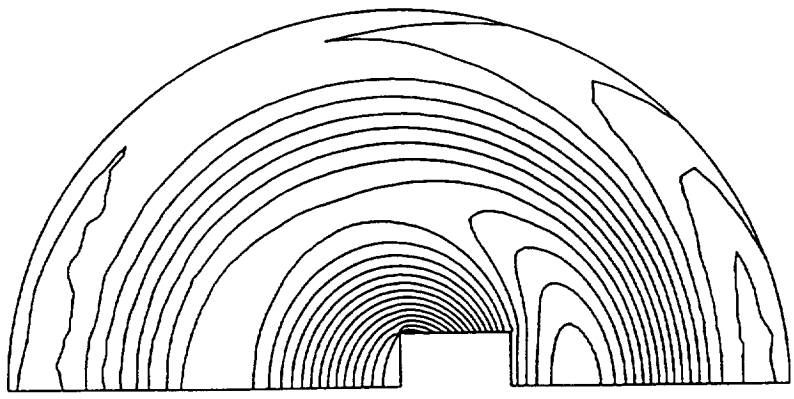

Figure 11 Scattered E_z contours for the square cylinder

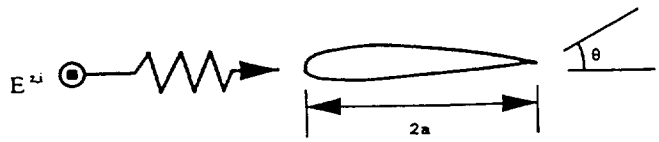

Figure 12 Scattering by a NACA0012 aerofoil: problem definition

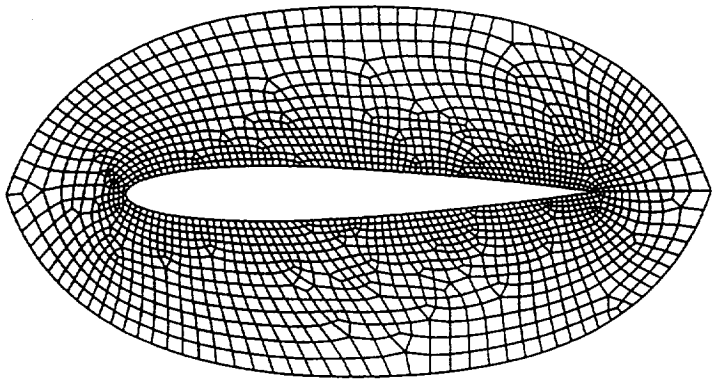

Figure 13 Scattering by a NACA0012 aerofoil: finite element mesh

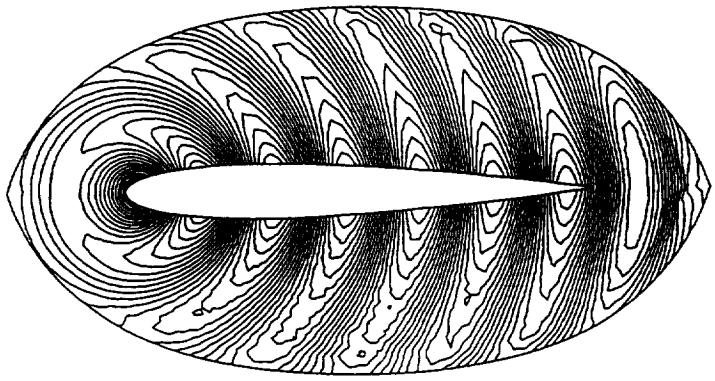

Figure 14 Scattered E_z contours for the NACA0012 aerofoil (0 degree incidence, $ka = 10$)

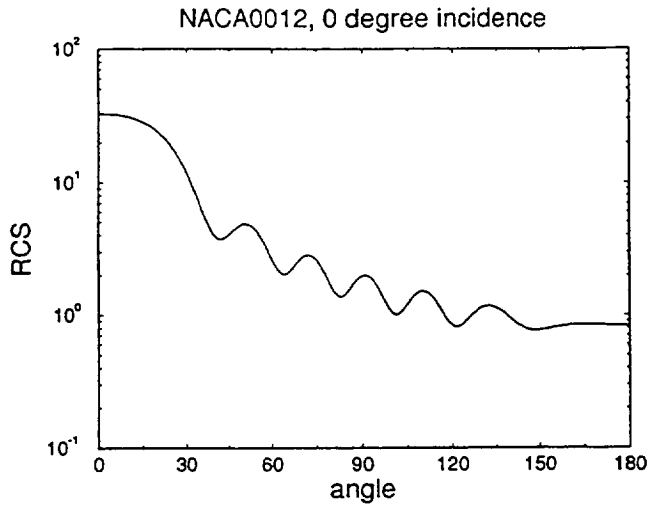

Figure 15 RCS for the NACA0012 airfoil (0 degree incidence, $ka = 10$)

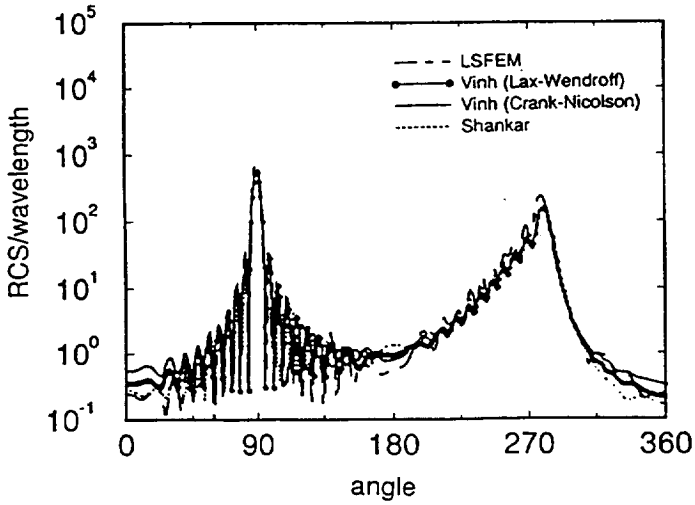

Figure 16 RCS for the NACA0012 airfoil (90 degree incidence, $ka = 10\pi$)

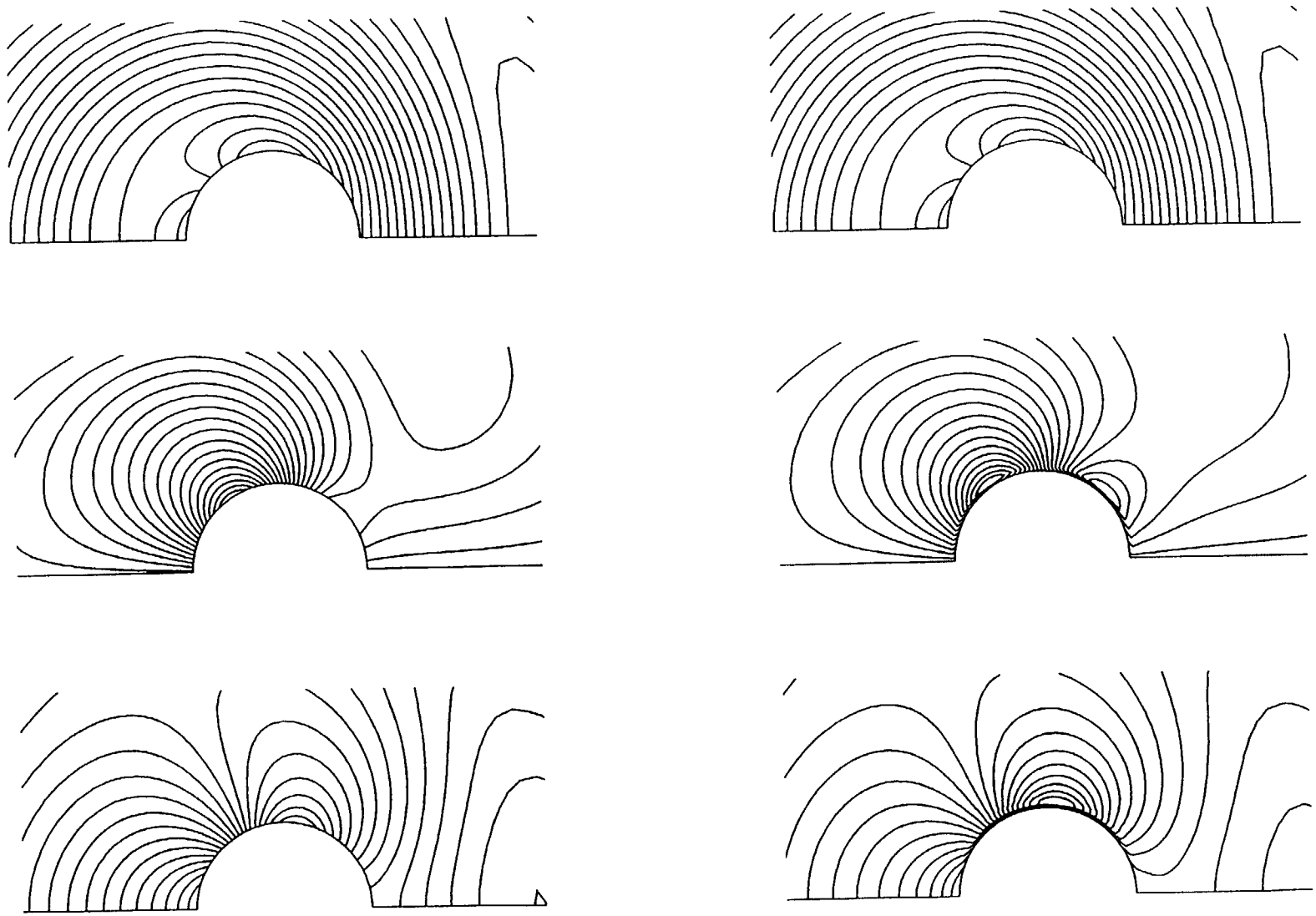

Figure 17 Comparison of the solution of the full Maxwell's equations (left) and the two curl equations(right), TM case, $ka = 1$, E_z, H_x, H_y respectively (top to bottom).

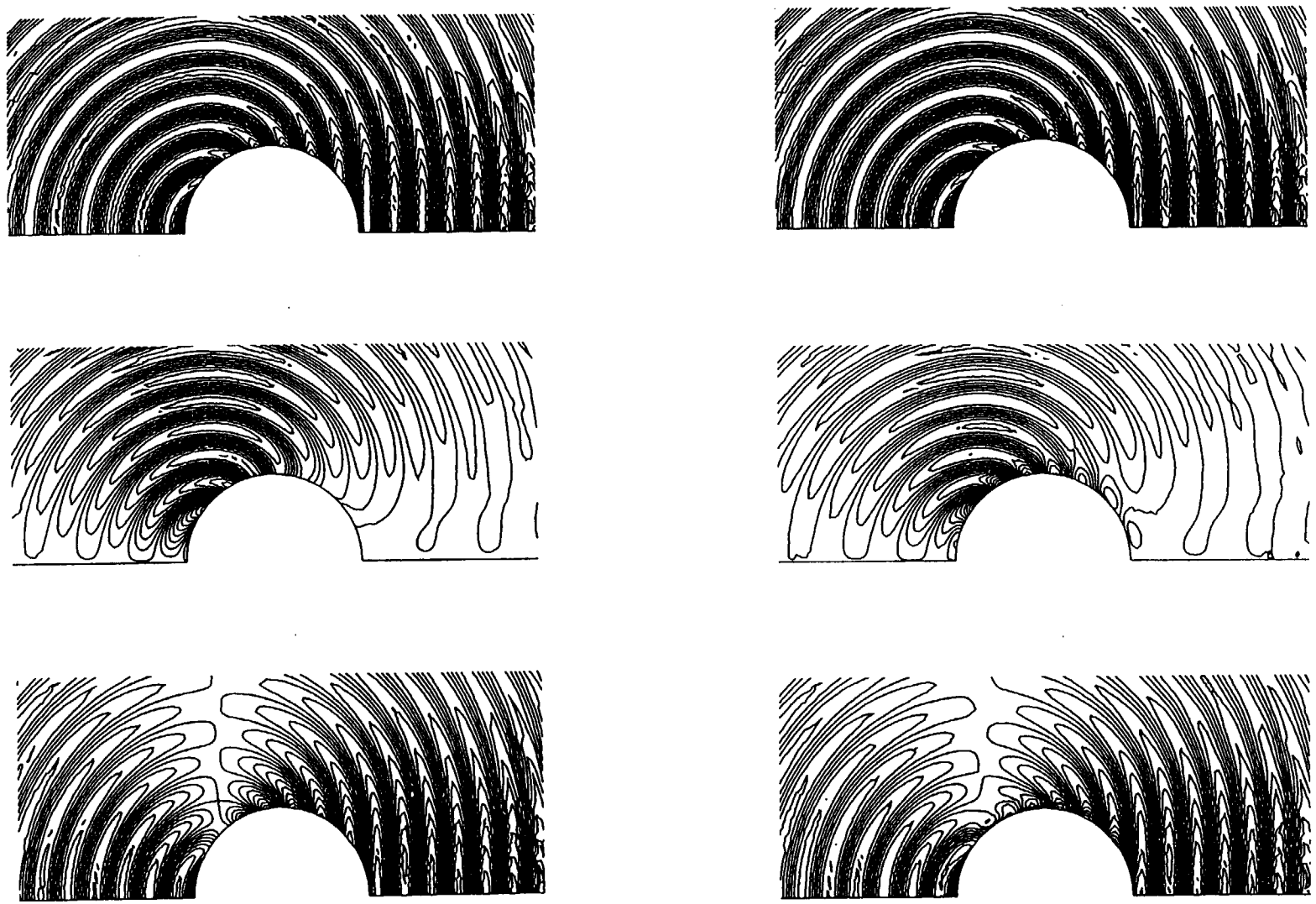

Figure 18 Comparison of the solution of the full Maxwell's equations (left) and the two curl equations(right), TM case, $ka = 10$, E_z, H_x, H_y respectively (top to bottom).

REPORT DOCUMENTATION PAGE

Form Approved
OMB No. 0704-0188

1. AGENCY USE ONLY (*Leave blank*)	2. REPORT DATE	3. REPORT TYPE AND DATES COVERED
	December 1996	Contractor Report

4. TITLE AND SUBTITLE

A Least-Squares Finite Element Method for Electromagnetic Scattering Problems

5. FUNDING NUMBERS

WU-505-90-5K
NCC3-483

6. AUTHOR(S)

Jie Wu and Bo-nan Jiang

7. PERFORMING ORGANIZATION NAME(S) AND ADDRESS(ES)

Institute for Computational Mechanics in Propulsion
22800 Cedar Point Road
Cleveland, Ohio 44142

8. PERFORMING ORGANIZATION REPORT NUMBER

E-10613

9. SPONSORING/MONITORING AGENCY NAME(S) AND ADDRESS(ES)

National Aeronautics and Space Administration
Lewis Research Center
Cleveland, Ohio 44135-3191

10. SPONSORING/MONITORING AGENCY REPORT NUMBER

NASA CR-202313
ICOMP-96-12

11. SUPPLEMENTARY NOTES

ICOMP Program Director, Louis A. Povinelli, organization code 2600, (216) 433-5818.

12a. DISTRIBUTION/AVAILABILITY STATEMENT

Unclassified - Unlimited
Subject Category 64

This publication is available from the NASA Center for AeroSpace Information, (301) 621-0390.

12b. DISTRIBUTION CODE

13. ABSTRACT ***(Maximum 200 words)***

The least-squares finite element method (LSFEM) is applied to electromagnetic scattering and radar cross section (RCS) calculations. In contrast to most existing numerical approaches, in which divergence-free constraints are omitted, the LSFEM directly incorporates two divergence equations in the discretization process. The importance of including the divergence equations is demonstrated by showing that otherwise spurious solutions with large divergence occur near the scatterers. The LSFEM is based on unstructured grids and possesses full flexibility in handling complex geometry and local refinement. Moreover, the LSFEM does not require any special handling, such as upwinding, staggered grids, artificial dissipation, flux-differencing, etc. Implicit time discretization is used and the scheme is unconditionally stable. By using a matrix-free iterative method, the computational cost and memory requirement for the present scheme is competitive with other approaches. The accuracy of the LSFEM is verified by several benchmark test problems.

14. SUBJECT TERMS

Least-squares; Finite element; Electromagnetics; Scattering; Radar cross section; Maxwell's equations; Divergence equation; Spurious solutions

15. NUMBER OF PAGES

35

16. PRICE CODE

A03

17. SECURITY CLASSIFICATION OF REPORT	18. SECURITY CLASSIFICATION OF THIS PAGE	19. SECURITY CLASSIFICATION OF ABSTRACT	20. LIMITATION OF ABSTRACT
Unclassified	Unclassified	Unclassified	